A&A 428, 511–521 (2004)
DOI: 10.1051/0004-6361:20048013

Astronomy & Astrophysics

The gas temperature in flaring disks around pre-main sequence stars⋆

B. Jonkheid[1], F. G. A. Faas[1], G.-J. van Zadelhoff[1,2], and E. F. van Dishoeck[1]

[1] Sterrewacht Leiden, PO Box 9513, 2300 RA Leiden, The Netherlands
e-mail: jonkheid@strw.leidenuniv.nl
[2] Royal Dutch Meteorological Institute, PO Box 201, 3730 AE De Bilt, The Netherlands

Received 2 April 2004 / Accepted 23 August 2004

Abstract. A model is presented which calculates the gas temperature and chemistry in the surface layers of flaring circumstellar disks using a code developed for photon-dominated regions. Special attention is given to the influence of dust settling. It is found that the gas temperature exceeds the dust temperature by up to several hundreds of Kelvins in the part of the disk that is optically thin to ultraviolet radiation, indicating that the common assumption that $T_{\rm gas} = T_{\rm dust}$ is not valid throughout the disk. In the optically thick part, gas and dust are strongly coupled and the gas temperature equals the dust temperature. Dust settling has little effect on the chemistry in the disk, but increases the amount of hot gas deeper in the disk. The effects of the higher gas temperature on several emission lines arising in the surface layer are examined. The higher gas temperatures increase the intensities of molecular and fine-structure lines by up to an order of magnitude, and can also have an important effect on the line shapes.

Key words. astrochemistry – stars: circumstellar matter – stars: pre-main sequence – molecular processes – ISM: molecules

1. Introduction

Circumstellar disks play a crucial role in both star and planet formation. After protostars have formed, part of the remnant material from the parent cloud core can continue to accrete by means of viscous processes in the disk (Shu et al. 1987). Disks are also the sites of planet formation, either through coagulation and accretion of dust grains or through gravitational instabilities in the disk (Lissauer 1993; Boss 2000). To obtain detailed information on these processes, both the dust and the gas component of the disks have to be studied. Over the last decades, there have been numerous models of the dust emission from disks, with most of the recent work focussed on flaring structures in which the disk surface intercepts a significant part of the stellar radiation out to large distances and is heated to much higher temperatures than the midplane (e.g. Kenyon & Hartmann 1987; Chiang & Goldreich 1997; D'Alessio et al. 1998, 1999; Bell et al. 1997; Dullemond et al. 2002). These models are appropriate to the later stages of the disk evolution when the mass accretion rate has dropped and the remnant envelope has dispersed, so that heating by stellar radiation rather than viscous energy release dominates. Such models have been shown to reproduce well the observed spectral energy distributions at mid- and far-infrared wavelengths for a large variety of disks around low- and intermediate-mass pre-main sequence stars.

Observations of the gas in disks started with millimeter interferometry data of the lowest transitions of the CO molecule (e.g. Koerner & Sargent 1995; Dutrey et al. 1996; Mannings & Sargent 1997; Dartois et al. 2003), but now also include submillimeter single-dish (e.g. Kastner et al. 1997; Thi et al. 2001; van Zadelhoff et al. 2001) and infrared (e.g. Najita et al. 2003; Brittain et al. 2003) data on higher excitation CO lines. Evidence for the presence of warm gas in disks also comes from near- and mid-infrared and ultraviolet observations of the H_2 molecule (e.g. Herczeg et al. 2002; Bary et al. 2003; Thi et al. 2001). Although emission from the hottest gas probed at near-infrared and ultraviolet wavelengths is thought to come primarily from a region within a few AU of the young stars, the longer wavelength data trace gas at larger distances from the star, >50 AU. Molecules other than CO are now also detected at (sub)millimeter wavelengths, including CN, HCN, HCO^+, CS and H_2CO (e.g. Dutrey et al. 1997; Kastner et al. 1997; Qi et al. 2003; Thi et al. 2004).

The emission from all of these gas tracers is determined both by their chemistry and excitation, where the latter depends on the temperature and density structure of the disk. The chemistry in flaring disks has been studied intensely in recent years by various groups (e.g. Aikawa et al. 1997; Willacy & Langer 2000; Markwick et al. 2002; van Zadelhoff et al. 2003), whereas the density structure is constrained from vertical hydrostatic equilibrium models of the dust disk assuming a contant gas/dust ratio (D'Alessio et al. 1999; Dullemond et al. 2002). In all of these models, the gas temperature is

⋆ Appendices are only available in electronic form at http://www.edpsciences.org

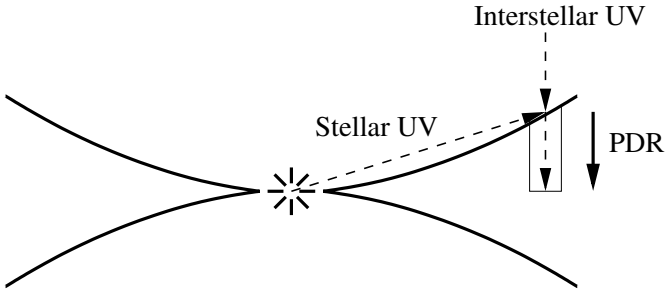

Fig. 1. The 1+1-D model. The disk is divided into annuli, each of which is treated as a 1-dimensional PDR problem for the chemistry and the cooling rates.

assumed to be equal to the dust temperature. That this assumption does not always hold was shown by Kamp & van Zadelhoff (2001), who calculated the gas temperature in tenuous disks around Vega-like stars. These disks have very low disk masses, of order a few $M_\oplus$, and are optically thin to ultraviolet (UV) radiation throughout. It was shown that their gas temperature is generally very different from the dust temperature, and that this higher temperature significantly affects the intensity of gaseous emission lines, in the most extreme cases by an order of magnitude or more (Kamp et al. 2003).

In this work, the gas temperature in the more massive disks (up to 0.1 $M_\odot$) around T-Tauri stars is examined, which are optically thick to UV radiation. Special attention is given to the effects of dust settling and the influence of explicit gas temperature calculations on the properties of observable emission lines.

The model used in this paper is described in Sect. 2. The resulting temperature, chemistry and emission lines are shown in Sect. 3. In Sect. 4 the limitations of our calculations are discussed, and in Sect. 5 our conclusions are presented. The details of the heating and cooling rates are in Appendices A and B, respectively.

2. Calculating the gas temperature

2.1. The PDR model

Because of the symmetry inherent in the disk shape, it is usually assumed that disks have cylindrical symmetry, resulting in a 2-dimensional (2-D) structure. Because of the computational problems in solving the chemistry (particularly the H_2 and CO self shielding) and cooling rates in a 2-D formalism, however, these are calculated by dividing the 2-D structure into a series of 1-D structures (see Fig. 1). The disk is divided into 15 annuli between 50 and 400 AU. These 1-D structures resemble the photon-dominated regions (PDRs) found at the edges of molecular clouds (for a review, see Hollenbach & Tielens 1997). A full 2-D formalism is used to calculate the dominant heating rates due to the photoelectric effect on Polycyclic Aromatic Hydrocarbons (PAHs) and large grains.

The 1-D PDR model described by Black & van Dishoeck (1987), van Dishoeck & Black (1988) and Jansen et al. (1995) is used in this work. This code consists of two parts: the first part calculates the photodissociation and excitation of H_2 in full detail, taking all relevant H_2 levels and lines into account. It includes a small chemical network containing the reactions relevant to the formation and destruction of H_2 to compute the H/H_2 transition. The main output from this code is the H_2 photodissociation rate as a function of depth and the fraction H_2^* of molecular hydrogen in vibrationally-excited states. The second part of the program includes a detailed treatment of the CO photodissociation process, a larger chemical network to determine the abundances of all species, and an explicit calculation of all heating and cooling processes to determine the gas temperature. The latter calculation is done iteratively with the chemistry, since the cooling rates depend directly on the abundances of O, C^+, C and CO. Each PDR consists of up to 130 vertical depth steps, with a variable step size adjusted to finely sample the important H→H_2 and C^+→C→CO transitions.

To simulate a circumstellar disk, some modifications had to be made in the PDR code. Because of the higher densities, thermal coupling between gas and dust had to be included. While this is not an important factor in most PDRs associated with molecular clouds, it dominates the thermal balance in the dense regions near the midplane of a disk. A variable density also had to be included to account for the increasing density towards the midplane of the disk. As input to the code, the density structure as well as the dust temperature computed by D'Alessio et al. (1999) are used. In this model, the structure is calculated assuming a static disk in vertical hydrostatic equilibrium. The disk is considered to be geometrically thin, so radial energy transport can be neglected. The model further assumes a constant mass accretion rate throughout the disk (a value of $\dot{M} = 10^{-8}\ M_\odot\ \mathrm{yr}^{-1}$ is used), and turbulent viscosity given by the α prescription ($\alpha = 0.01$). In the outer disk studied here, the contribution of accretion to the heating is negligible. The central star is assumed to have a mass of 0.5 $M_\odot$, a radius of 2 $R_\odot$ and a temperature of 4000 K. The disk mass is 0.07 $M_\odot$ and extends to ∼400 AU. This same model has been used by Aikawa et al. (2002) and van Zadelhoff et al. (2003) to study the chemistry of disks such as that toward LkCa 15 and TW Hya. As shown in those studies, the results do not depend strongly on the precise model parameters.

Further input to the PDR code is the strength of the UV field. The UV field is based on the spectrum for TW Hya obtained by Costa et al. (2000) (stellar spectrum B in van Zadelhoff et al. 2003): a 4000 K black body spectrum, plus a free-free and free-bound contribution at 3×10^4 K and a 7900 K contribution covering 5% of the central star. The intensities of the resulting UV radiation incident on the disk surface at each annulus (with both a stellar and an interstellar component) are calculated using the 2-D Monte Carlo code of van Zadelhoff et al. (2003). The resulting UV intensities are then converted into a scaling factor I_{UV} with respect to the standard interstellar radiation field as given by Draine (1978). These scaling factors I_{UV} form the input to calculate the chemistry for each of the 15 vertical PDRs and range from ∼1000

Table 1. Adopted gas-phase elemental abundances with respect to hydrogen.

Element	Abundance
D	1.5×10^{-5}
He	7.5×10^{-2}
C	7.9×10^{-5}
N	2.6×10^{-5}
O	1.8×10^{-4}
S	1.7×10^{-6}
PAH	1.0×10^{-7}

at the first slice at 63 AU to ∼100 at the last slice at 373 AU. As shown by van Zadelhoff et al. (2003), the difference in the chemistry calculated with spectrum B and a scaled Draine radiation field (spectrum A) is negligible. It is important to note that both radiation fields have ample photons in the 912–1100 Å regime which are capable of photodissociating H_2 and CO and photoionizing C.

The UV radiation also controls the heating of the gas through the photoelectric effect on grains and PAHs. The rates of these two processes are calculated using the 2-D radiation field at each radius and height in the disk computed by van Zadelhoff et al. (2003) including absorption and scattering.

2.2. Chemistry

To calculate the chemistry, the network of Jansen et al. (1995) is used. It contains 215 species consisting of 26 elements (including isotopes) with 1549 reactions between them. The adopted abundances of the most important elements are shown in Table 1; the carbon and oxygen abundances are similar to those used by Aikawa et al. (2002). The chemistry has been checked against updated UMIST databases, but only minor differences have been found for the species observed in PDRs. Since the temperature depends primarily on the abundances of the main coolants, the precise chemistry does not matter as long as the $C^+ \rightarrow C \rightarrow CO$ transition is well described. The adopted cosmic ray ionization rate is $\zeta = 5 \times 10^{-17}$ s^{-1}.

Since the chemical timescales in the PDR layer are short (at most a few thousand yr) compared to the lifetime of the disk, the chemistry is solved in steady-state. Only gas-phase reactions are considered; no freeze-out onto grains is included. Accordingly, the PDR calculations are stopped when the dust temperature falls below 20 K. Since this is also the regime where the gas and dust are thermally coupled (see Sect. 3.1), no explicit calculation of the gas temperature is needed.

It should be noted that only the vertical attenuation is considered here in the treatment of the photorates used in the chemistry, in contrast to the work by Aikawa et al. (2002) who included attenuation along the line of sight to the star. This means that the photorates are generally larger deeper into the disk. This is illustrated in Fig. 2, where the dissociation rate of C_2H is shown as a function of height. Comparison with the rate found by van Zadelhoff et al. (2003) shows that the dissociating radiation penetrates deeper (to a height of ∼40 AU opposed to ∼60 AU) into the disk. Given the overall uncertainties in the radiation field and disk structure these effects are not very significant. Another difference of our model with those of Aikawa et al. (2002) and van Zadelhoff et al. (2003) is the full treatment of CO photodissociation as given by van Dishoeck & Black (1988), including self shielding and the mutual shielding by H_2.

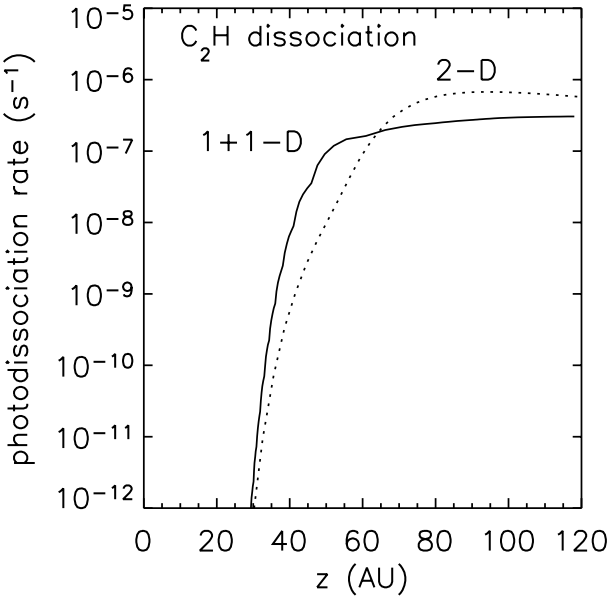

Fig. 2. The photodissociation rate of C_2H at a radius of 105 AU. The solid line gives the rate found in this work, the dotted line the rate by van Zadelhoff et al. (2003).

2.3. Thermal balance

The gas temperature in the disk is calculated by solving the balance between the total heating rate Γ and the total cooling rate Λ. The equilibrium temperature is determined using Brent's method (Press et al. 1989). Heating rates included in the code are due to the following processes: photoelectric effect on PAHs and large grains, cosmic ray ionization of H and H_2, C photoionization, H_2 formation, H_2 dissociation, H_2 pumping by UV photons followed by collisional de-excitation, pumping of [O I] by infrared photons followed by collisional de-excitation, exothermic chemical reactions, and collisions with dust grains when $T_{\rm dust} > T_{\rm gas}$. The gas is cooled by line emission of C^+, C, O and CO, and by collisions with dust grains when $T_{\rm dust} < T_{\rm gas}$. A detailed description of each of these processes is given in Appendix A. The thermal structure found in our PDR models has been checked extensively against that computed in other PDR codes.

There are two important assumptions in our calculation of the thermal balance which may not necessarily be valid for disks compared with the traditional PDRs associated with molecular clouds. The first is the use of a 1-D escape probability method for the cooling lines. This limitation is further discussed in Sect. 4.1. The second is the assumption that the photoelectric heating efficiency for interstellar grains also holds

for grains in disks. As shown by Kamp & van Zadelhoff (2001), this efficiency is greatly reduced if the grains have grown from the typical interstellar size of 0.1 μm to sizes of a few μm. While there is good observational evidence for grain growth for older, tenuous disks, the younger disks studied here are usually assumed to have a size distribution which includes the smaller grains.

2.4. Dust settling

In turbulent disks, the gas and dust are generally well-mixed. Stepinski & Valageas (1996) have shown that the velocities of dust grains with sizes <0.1 cm are coupled to the gas. When the disk becomes quiescent, models predict that dust particles are no longer supported by the gas and will start to settle towards the midplane of the disk (Weidenschilling 1997). During the settling process, dust particles will sweep up and coagulate other dust particles, thus leading to grain growth. Since larger particles have much shorter settling times than small particles, coagulation accelerates the settling process.

Observational evidence for dust growth and settling in disks includes the near-IR morphology of the edge-on disks. For example, for the 114–526 disk in Orion, Throop et al. (2001) and Shuping et al. (2003) show that the large dust grains in this disk are concentrated in the midplane. The SEDs of some of the T-Tauri stars examined by Miyake & Nakagawa (1995) also indicate that dust settling takes place, as well as the statistics of observations of edge-on disks by D'Alessio et al. (1999).

In our model, dust settling is simulated by varying the gas/dust mass ratio. In this paper, both models with a constant $m_{\rm gas}/m_{\rm dust}$ ("well-mixed") and a variable value of $m_{\rm gas}/m_{\rm dust}$ ("settled") are presented. In the well-mixed case, the gas/dust mass ratio is taken to be 100 throughout. For the settled model, the value of 100 is kept near the midplane of the disk, while a value of 10^4 is used in the surface regions. The precise value adopted at the surface is not important, as long as it is high enough that photoelectric heating is no longer significant in this layer. The ratio is varied linearly with depth in a narrow transition region. The boundaries of the transition region are defined as $z_6 \pm h/10$, where z_6 is the height where the settling time of dust particles is 10^6 years (this method thus simulates a disk that is 10^6 years old) and h is the height of the D'Alessio disk, defined as the height where the gas pressure is equal to 7.2×10^5 K cm^{-3}.

The settling time $t_{\rm settle}$ is determined as follows:

$$t_{\rm settle} = \frac{z}{v_{\rm settle}}$$

where z is the height above the midplane. The settling velocity $v_{\rm settle}$ is determined by the balance between the vertical component of the gravitational force on the dust grains and the drag force the grain experiences as it moves through the gas. For the drag force the subsonic limit of the formulae by Berruyer (1991) is used, resulting in a settling velocity of

$$v_{\rm settle} = \frac{\sqrt{\pi}\, G\, M\, z\, a\, \rho}{2\, r^3\, \mu\, n_{\rm H}\, v_{\rm thermal}}$$

with G the gravitational constant, M the stellar mass, a the grain radius (a typical value of 0.1 μm is used), ρ the density of the grain material (2.7 g cm^{-3}), $r = \sqrt{z^2 + R^2}$ the distance from the star, μ the mean molecular weight (2.3 proton masses) and $v_{\rm thermal}$ the thermal velocity of the gas particles ($v_{\rm thermal} = \sqrt{2\,k\,T/\mu}$). The settling times found by this method are displayed in Fig. 3.

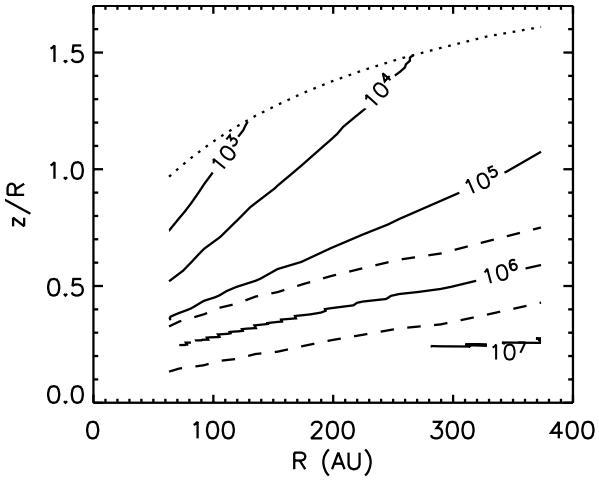

Fig. 3. Settling times in years for 0.1 μm-sized dust particles. The dashed lines give the boundaries between which the $m_{\rm gas}/m_{\rm dust}$ ratio is interpolated from a value of 10^4 to 10^2.

It is further assumed that the smallest particles represented by PAHs remain well-mixed with the gas in all models considered here. Observations show evidence for PAH emission from disks, at least around Herbig Ae stars (e.g. Meeus et al. 2001), whereas detailed models indicate that their settling times are much longer than the ages of the disks (Weidenschilling 1997). This means that PAH heating is still at full strength in the upper layers of the disk while photoelectric heating on large grains is suppressed in the case of dust settling. The PAHs are also responsible for approximately half of the absorption of UV radiation with wavelengths shorter than 1500 Å which dissociates molecules (e.g. Li & Greenberg 1997). Thus, much of the UV radiation which affects the chemistry is still absorbed in the upper layers even when large dust particles are settling. In our models, this is taken into account by adopting an effective $A_{\rm V}$ in the calculation of the depth-dependent photodissociation rates. Specifically, the gas/dust parameter $x_{\rm gd}$ is defined as the actual value of the $m_{\rm gas}/m_{\rm dust}$ divided by the interstellar value. Thus, $x_{\rm gd}$ varies between 1 and 100. The visual extinction then becomes

$$A_{\rm V} = \left(\frac{N_{\rm H}}{1.59 \times 10^{21}\ {\rm cm}^{-2}}\right) \times \frac{1}{x_{\rm gd}}.$$

The effective extinction used for photorates at UV wavelengths

$$A_{\rm V,eff} = \left(\frac{N_{\rm H}}{1.59 \times 10^{21}\ {\rm cm}^{-2}}\right) \times \frac{1}{2}\left(\frac{1}{x_{\rm gd}} + 1\right).$$

Thus the dissociating radiation is still reduced (albeit at half strength) in areas where large grains have disappeared completely.

The scaling of the various heating and cooling rates in the settling model is described in Appendix A. In particular,

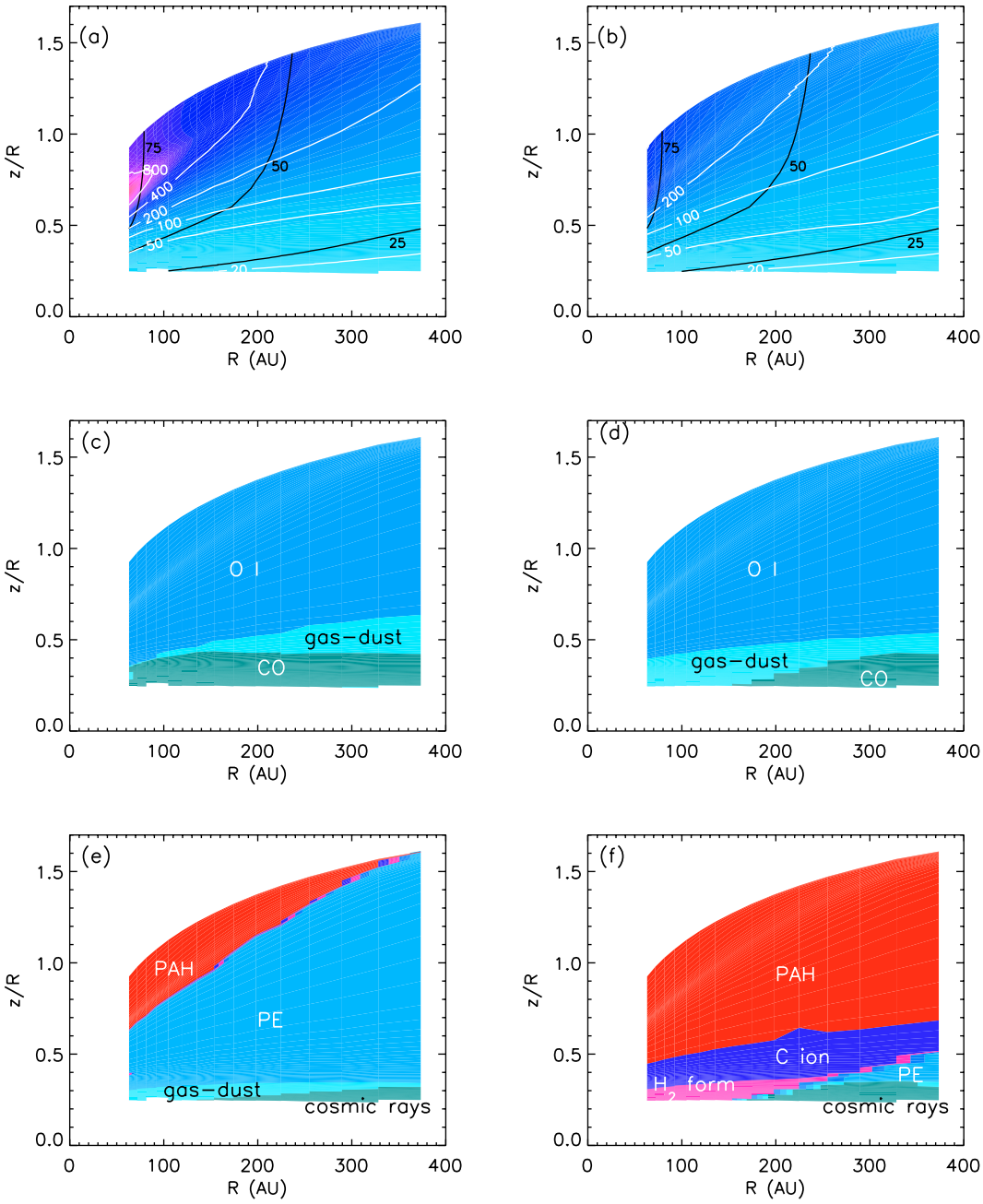

Fig. 4. The temperature structure of the disk. The colorscale and the white contours give the gas temperature, the black contours give the dust temperature for the well-mixed model **a)** and the dust settling model **b)**. The dominant cooling rates are also shown for the well-mixed **c)** and settled **d)** models, as well as the dominant heating rates in **e)** and **f)**.

it should be noted that although the H_2 grain surface formation rate is reduced, H_2 formation through the reaction PAH:H + H → PAH + H_2 is included in the chemical network. Since this reaction has a rate comparable to the H_2 formation rate on large grains the abundance of H_2 is lowered by only a factor of 2 in the upper layers if the settled disk. If H_2 formation through PAHs is excluded, the H → H_2 transition occurs deeper in the disk, but the effect on the C^+ → C → CO transition is small. The overall gas density structure is kept the same as in the well-mixed model, as is the dust temperature distribution. The latter assumption is certainly not valid, but since gas-dust coupling only plays a role in the lower layers, this does not affect our results.

3. Results

3.1. Temperature

The results of the temperature calculations are presented in Fig. 4 for the entire disk, and in Fig. 5 for a vertical slice through the disk at 105 AU. It can be seen that the vertical temperature distribution resembles that of a "normal" PDR (see

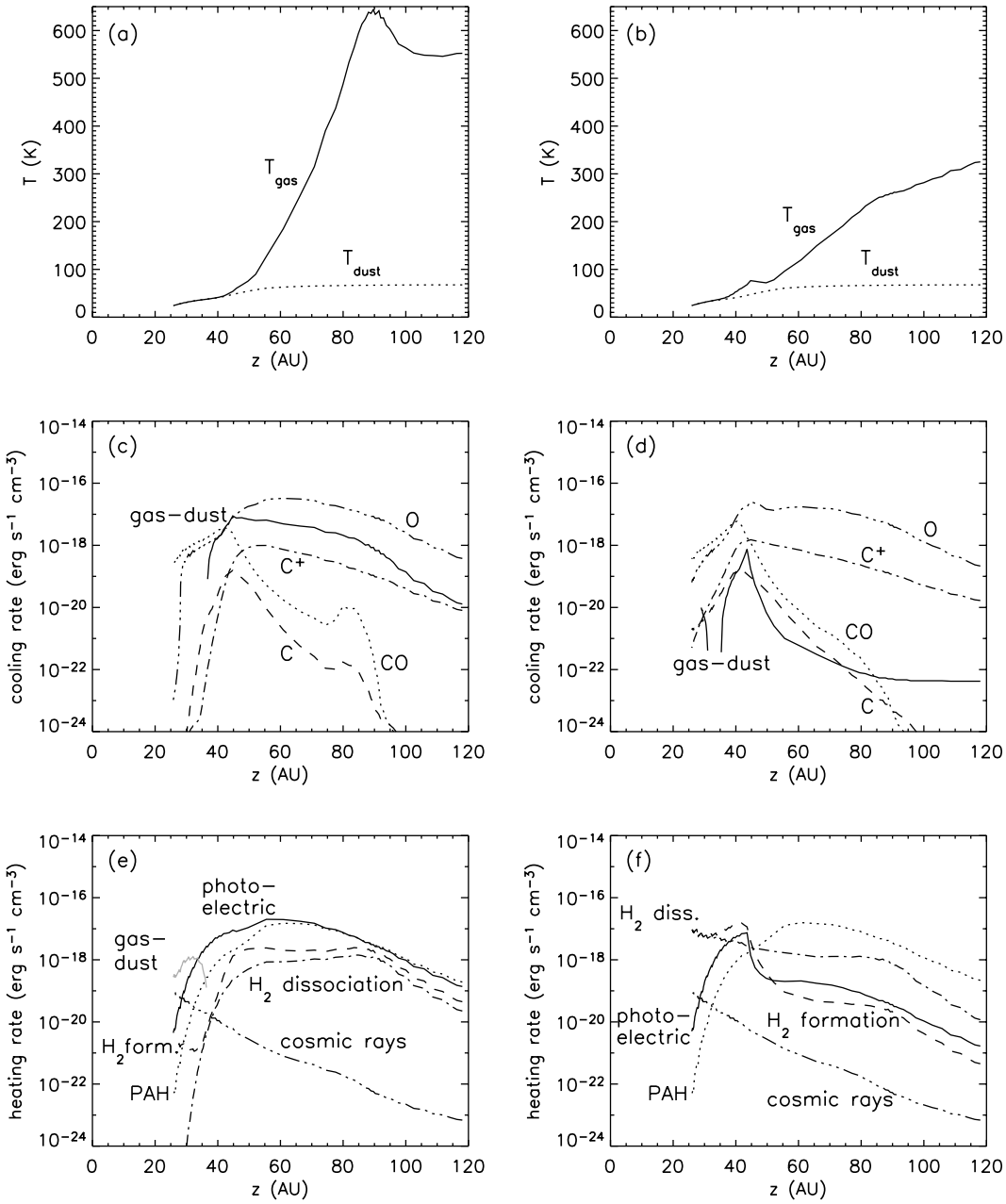

Fig. 5. The vertical temperature distribution at a radius of 105 AU for the well-mixed **a)** and the settled **b)** models. Figures **c)** and **d)** give the cooling rates at this radius, where the solid line denotes cooling by gas-dust collisions, the dashed line [C I] cooling, the dotted line CO cooling, the dash-dot line [C II] cooling and the dash-triple dot line [O I] cooling. Figures **e)** and **f)** give the heating rates: the solid line gives the photoelectric heating rates on large grains, the dotted line on PAHs; the dashed and dash-dot lines gives the heating rates due to the formation and dissociation of H_2, respectively, the dash-triple dot line gives the cosmic ray heating rate, and the grey solid line gives the heating rate due to gas-grain collisions.

for example Tielens & Hollenbach 1985): the gas temperature is much higher than the dust temperature at the disk surface, and both temperatures decrease with increasing visual extinction. In annuli close to the central star the surface temperatures go up to 1000 K. The precise temperature in these annuli is uncertain and depends on the adopted molecular parameters. For example, when the H_2^* vibrational de-excitation rate coefficients given by Tielens & Hollenbach (1985) are used, the rate increases steeply with increasing temperature with the cooling rate unable to keep up, resulting in a numerical instability in the code. When the rate coefficients given by Le Bourlot et al. (1999) are used, a stable temperature can be found.

The main difference between the temperature structures in disks and general molecular clouds is caused by the increasing density in disks: in standard PDRs the density generally stays uniform, causing the gas temperature to fall below the dust temperature at high optical depths. In disks, the increasing density causes the coupling between gas and dust to dominate the thermal balance in the deeper layers, so that the gas temperature becomes equal to the dust temperature.

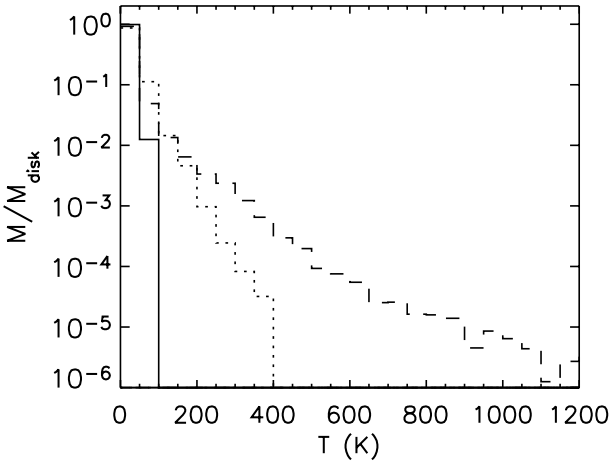

Fig. 6. The normalized distribution of the temperature over total disk mass. The solid line shows the dust temperature, the dashed line the gas temperature of the well-mixed model, and the dotted line the gas temperature of the settled model.

The normalized distribution of the gas temperature over the disk mass between 63 AU and 373 AU of the central star is shown in Fig. 6. The calculations are performed down to a dust temperature of ~20 K. It can be seen that even though the bulk of the gas mass is at the same temperature as the dust, a considerable fraction (~10%) in the surface layers is at higher temperatures, especially in the case of dust settling. Since most of the molecular emission arises from this layer, the difference is significant. It can also be seen that the settled model contains the largest amount of hot gas, even though the maximum temperature is higher in the well-mixed case.

The above figures illustrate that $T_{\rm gas} = T_{\rm dust}$ is invalid in the upper layers of the disk. This can also be seen in the individual heating and cooling rates in Fig. 5: gas-dust collisions dominate the heating/cooling balance only deep within the disk. In the upper layers the heating due to the photoelectric effect on large grains and PAHs is so large that cooling of the gas through collisions with dust grains is not effective anymore, and atomic oxygen becomes the dominant cooling agent. This shifts the equilibrium to higher gas temperatures.

In the case of dust settling, the photoelectric effect on large grains and the H_2 formation heating rates are suppressed by a factor of 100. The PAH heating is still effective, resulting in a temperature that is ~50% lower than in the well-mixed model. In this model there is also less absorption of UV radiation in the upper layers, resulting in higher temperatures deeper in the disk compared to the well-mixed model. When the abundance of large grains rises, all this UV radiation is available for photoelectric heating, resulting in a peak in the gas temperature. This extra UV is rapidly absorbed here, causing a sudden drop in the temperature as gas-dust collisions become the dominant process in the thermal balance. If the PAHs are removed from the model, thus simulating a disk where these small grains have disappeared, the temperature in the outer regions drops even further, but the overall shape of the temperature structure does not change much.

3.2. Chemistry

In Figs. 7 and 8 the chemical structure of the disk is presented. The chemistry follows that of an ordinary PDR: a region consisting mainly of atomic H in the outer layers, with a sharp transition to the deeper molecular layers. Self-shielding of H_2 quickly reduces the photodissociation rate, so the deeper layers consist mainly of molecular hydrogen. The principle carbon-bearing species follow a similar trend, consisting mainly of C^+ in the upper layers, with a transition to C, and later CO, at larger optical depths. In the deeper layers CO is also protected from dissociation by self-shielding and by shielding by H_2, as several dissociative wavelengths overlap for these molecules. Because CO is much less abundant than H_2, absorption by dust also plays an important role in decreasing its dissociation rate. This causes the carbon in the disk to be mostly ionic in the upper layers, and mostly molecular (in the form of CO) deeper in the disk. Compared with the models of Aikawa et al. (2002) and van Zadelhoff et al. (2003), our C → CO transition occurs somewhat deeper into the disk, at $z \sim 40$ AU rather than 60 AU for the $R = 105$ AU annulus. This is due to the geometry in the 1+1-D model, which allows dissociating radiation to penetrate more deeply into the disk, as well as our different treatment of CO photodissociation.

In the case of dust settling the C^+/C/CO transition occurs slightly deeper in the disk. This is explained by the higher photodissociation rates deeper in the disk due to the decreased absorption of UV radiation by large dust grains. The PAHs in the outer regions still absorb a significant fraction of the UV, so the effect is not very large. Since the H/H_2 transition is determined by H_2 self shielding and not dust absorption, the position of this transition does not change if the dust settles.

The chemistry has also been calculated for a model where $T_{\rm gas} = T_{\rm dust}$. It is found that the different temperature has little effect on the abundances of those species important in the thermal balance. The chemistry in the surface layers of disks is mostly driven by photo-reactions and ion-molecule reactions, both of which are largely independent of temperature.

3.3. Line intensities

The main effect of the high gas temperatures is on the intensities and shapes of emission lines arising from the warm surface layers. It is expected that the intensities of lines tracing high temperatures (such as the [O I] fine-structure lines, the H_2 rotational lines, and the higher CO rotational lines) will increase due to the higher temperatures, and the larger overall amount of warm gas.

The model line profiles are created using the 2-D Monte Carlo code by Hogerheijde & van der Tak (2000) assuming a Keplerian velocity field and an inclination of 60°. The results for the [C I], [O I] and [C II] fine-structure lines and the rotational lines of CO are shown in Fig. 9. It can be seen that the high gas temperatures have a significant impact on the intensities, and particularly on the [O I] and [C II] fine-structure lines. The difference in the locations in the disk where these lines are predominantly excited is reflected in the different shapes of the lines. The lines tracing hot gas all

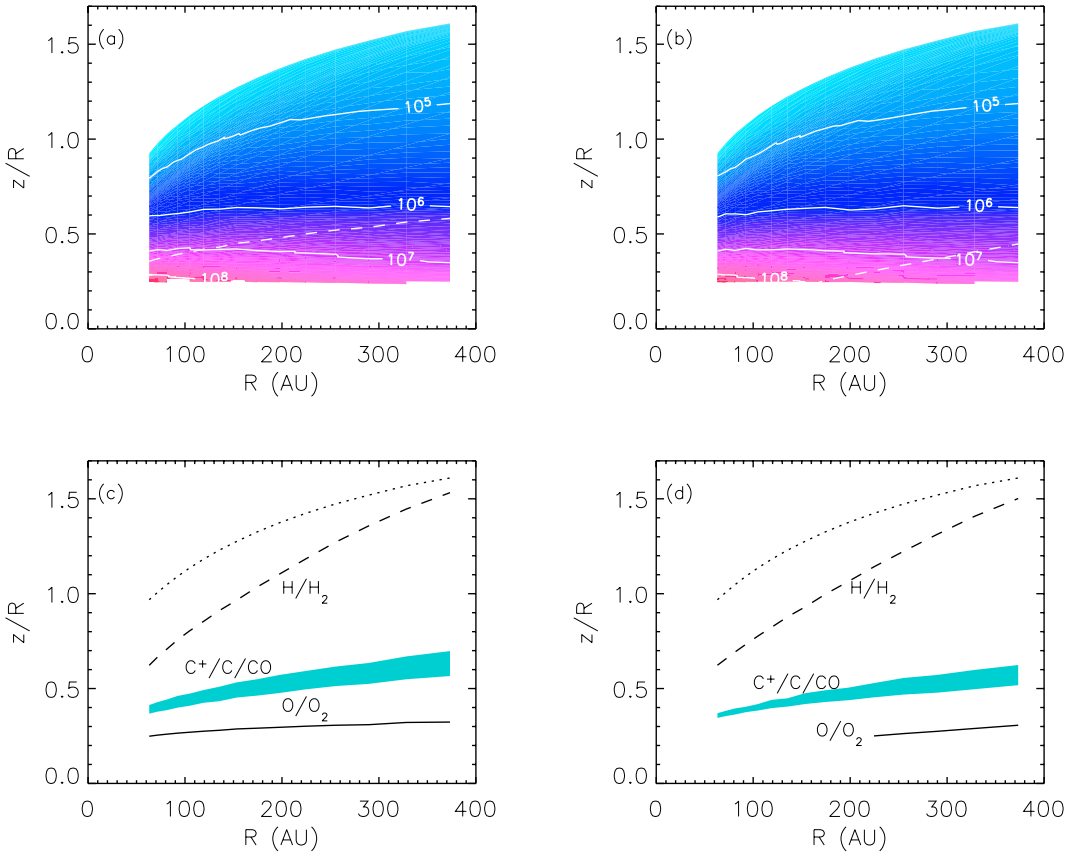

Fig. 7. Chemical abundances for the well-mixed (*left column*) and settled (*right column*) models. In **a)** and **b)**, the density profile of the disk is shown, as well as the $A_V = 1$ surface denoted by the dashed line. In **c)** and **d)**, the surface of the disk is shown as a dotted line, the H/H_2 transition as a dashed line, and the O/O_2 transition as a solid line. The shaded area denotes the C^+/C/CO transition.

display a double-peaked structure, due to their excitation in the innermost parts of the disk. It can also be seen that the higher gas temperature has little effect on the lower rotational lines of CO and the lowest [C I] fine-structure line. These lines trace the cold gas, which is present in the deeper layers of the disk in all models.

4. Discussion

4.1. Limitations of the 1+1-D model

While circumstellar disks are inherently 2-dimensional structures, a complete 2-D treatment of the radiative transfer, chemistry and thermal balance is at present too time-consuming to be practical. The 1+1-D model circumvents this problem by drastically simplifying the geometry to a series of 1-D structures. The main disadvantage of the 1+1-D model is its poor treatment of radiative transfer: in principle, only transfer in the vertical direction is included. In a pure 1+1-D geometry the stellar radiation is forced to change direction when it hits the disk's surface and thus affects the chemistry calculation. This problem does not apply to the photoeletric heating rates of PAHs and large grains since they were calculated using a UV field calculated with the 2-D Monte Carlo code by van Zadelhoff et al. (2003).

The 1+1-D geometry also affects the escape probabilities of the radiative cooling lines, which have to travel vertically instead of escaping via the shortest route to the disk's surface. Thus the escape probabilities calculated by the 1+1-D model are generally too low.

The overall effect of the 1+1-D geometry on the disk temperature is subtle: the very upper layers of the disk are optically thin regardless of the adopted geometry, so the temperature and chemistry results are expected to be correct there. In the dense regions near the midplane, the dust opacities are so large that there will be little effect of the geometry either. Also, due to the strong thermal coupling between gas and dust, the gas temperature is equal to the dust temperature there. The greatest uncertainties are in the chemistry, in the intermediate regions between the surface and the midplane. Since the thermal balance is tied to the chemistry, it is expected that the largest uncertainties in the gas temperature occur also in this region. It should be noted that many secondary effects play a role here, including the precise formulation of the cooling rates, treatment of chemistry, self-shielding, etc. The current models should be adequate to capture the main characteristics and magnitude of all of these effects.

4.2. Effects of gas-dust coupling

It can be seen in Fig. 10 that thermal coupling between gas and dust has a small effect on the gas temperature in the upper layers of the disk: the gas temperature is so high and

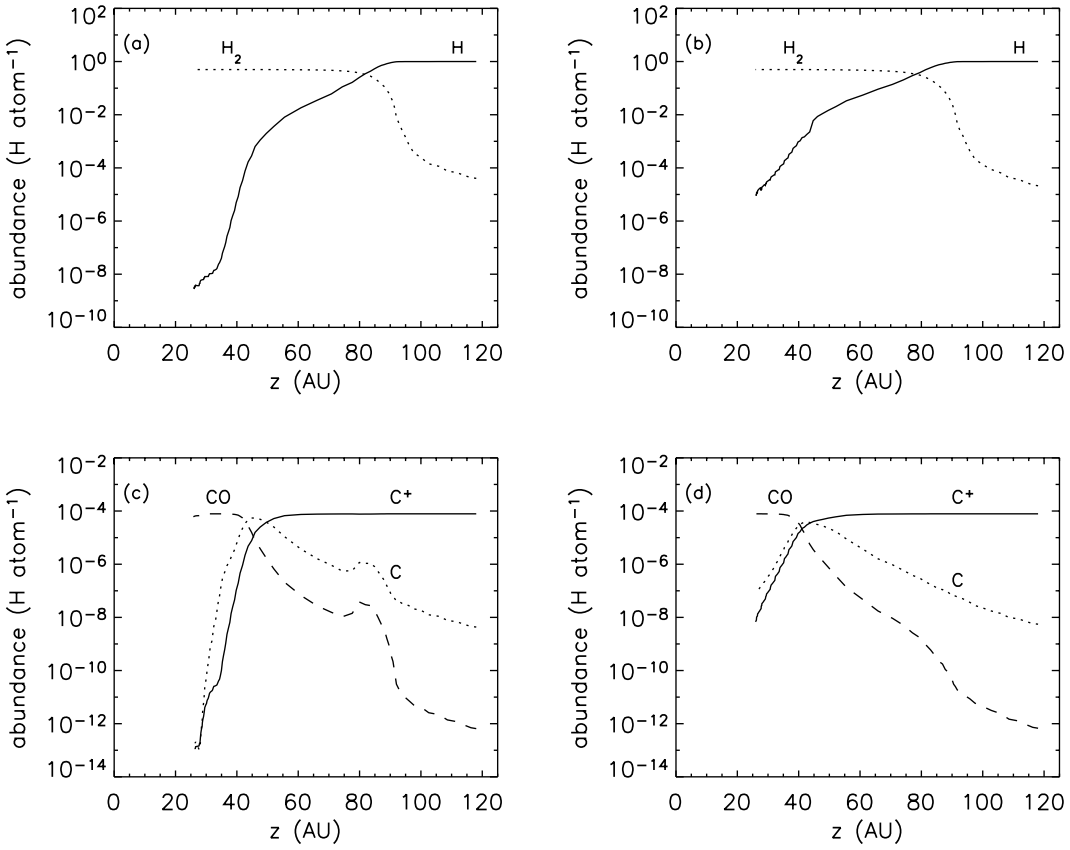

Fig. 8. The vertical distribution of several chemical species in the disk at 105 AU for the well-mixed (*left column*) and settled (*right column*) models. Figures **a)** and **b)** show the abundances of H and H_2; Figs. **c)** and **d)** of C^+, C and CO.

density comparitively low that gas-dust collisions are an ineffective cooling mechanism. Deeper in the disk the coupling becomes stronger and eventually comes to dominate the thermal balance. The overall effect on the resulting temperature is small because gas and dust already have similar temperatures even when the coupling is ignored.

4.3. Effects of the radiation field

The radiation field used in this work is assumed to have the same spectral shape as the Draine (1978) field with integrated intensity matched to the observed radiation field of TW Hya (Costa et al. 2000). Bergin et al. (2003) have shown that this treatment may overestimate the amount of radiation in the 912–1100 Å regime where H_2 and CO are dissociated, since a significant fraction of the UV flux is in emission lines (particularly Ly α). Thus the dissociation rates of H_2 and CO, as well as the C ionization rate may be too high in this work. Other molecules such as H_2O and HCN, however, have significant cross sections at Lyα.

If the radiation field of Bergin et al. (2003) is used, the chemistry of the relevant cooling species will become more similar to that found using spectrum C (a 4000 K blackbody) in van Zadelhoff et al. (2003). Because of the different chemistry, it is also expected that the temperature profile will change: CO will become the dominant carbon-bearing species at larger heights, where it can cool the gas more efficiently. It is therefore expected that the temperature in the intermediate layers will drop with respect to the results presented here. The heating rates are not sensitive to changes in the chemistry, so they will not change much.

5. Conclusions

The main conclusions of our calculations are:

- The gas temperature is much higher than the dust temperature in the optically thin part of the disk, while the two temperatures are the same in the part of the disk which is optically thick to UV radiation and where most of the disk's material resides.
- The temperatures in the optically thin part have a noticeable effect on the excitation of higher-lying emission lines. The higher temperatures should also affect the disk's structure: since the structure is calculated assuming hydrostatic equilibrium, the high temperatures in the surface regions will blow-up the disk, which will achieve hydrostatic equilibrium at a greater height. This in turn will lead to a more efficient outgassing of the disk. An initial discussion of this effect is given in Kamp & Dullemond (2004).
- The chemistry in the disk does not change much when the gas temperature is increased in the explicit calculation.
- Dust settling is found to have a great impact on the gas temperature in the disk. The gas temperature in disks where settling is taking place is found to be lower, and decreases less

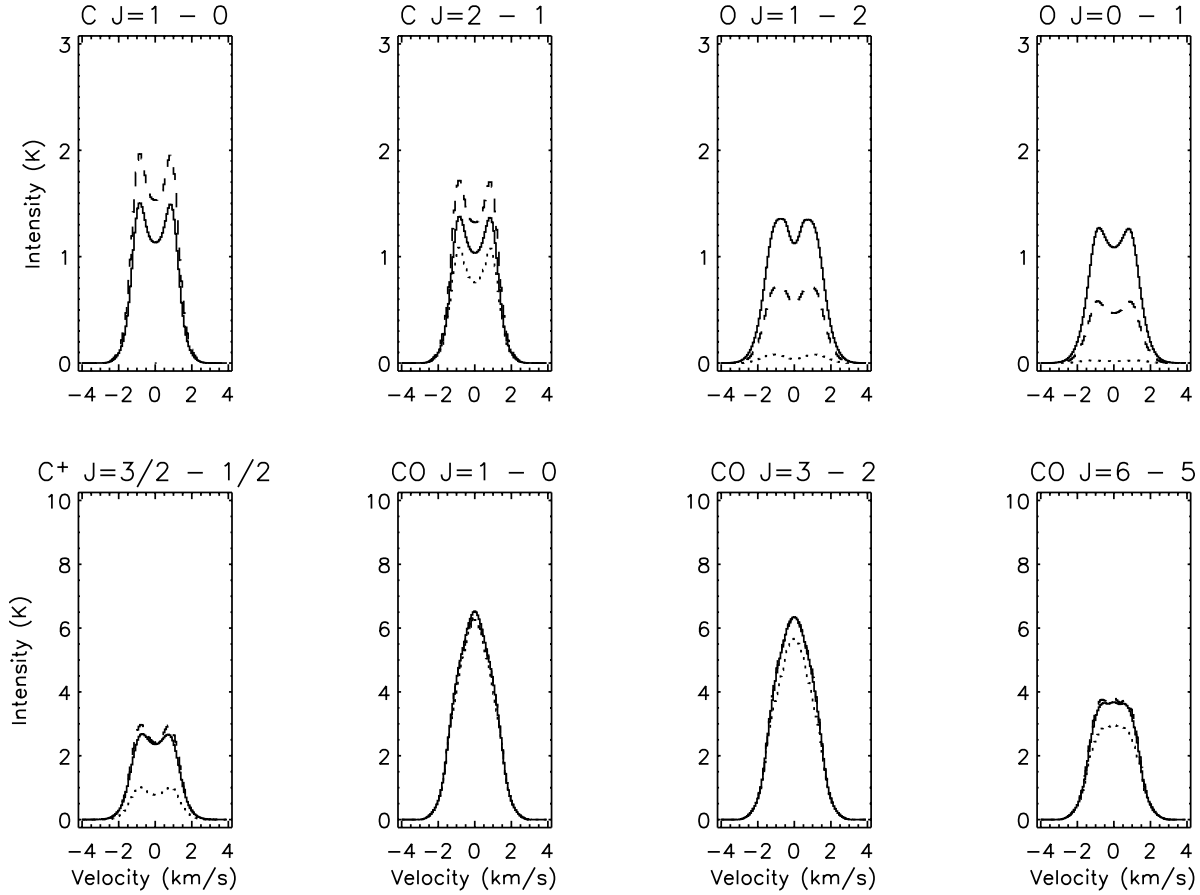

Fig. 9. The emission lines of C, O, C^+ and CO for three scenarios: $T_{\rm gas} = T_{\rm dust}$ (dotted line), and $T_{\rm gas}$ calculated explicitly in the well-mixed (solid line) and settled (dashed line) model. Units are in Kelvins, assuming that the disk fills the beam precisely; this corresponds to a beam size of 5″ when the disk is at 150 pc.

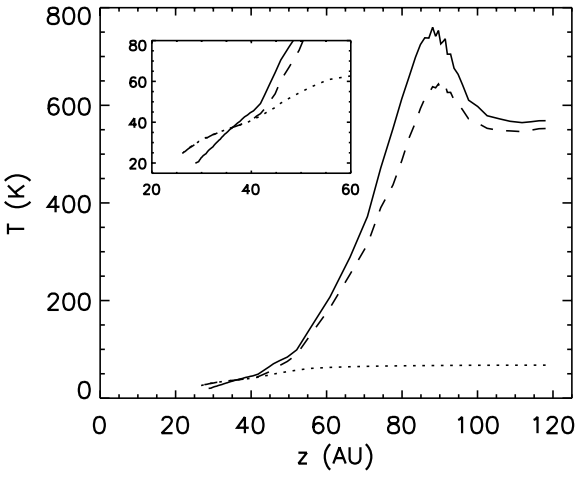

Fig. 10. Vertical distribution of gas and dust temperatures in the disk at a radius of 105 AU. The solid line gives the gas temperature when gas-dust collisions are ignored, the dashed line gives the gas temperature when these collisions are included in the thermal balance. The dotted line gives the dust temperature. The inset shows the region around $T_{\rm gas} = 20$ K.

steeply than in well mixed disks. Due to the lower temperatures, the intensities of higher-lying lines are lower than in well mixed disks.

– Dust settling does not greatly affect the disk's chemistry. This is because PAHs are assumed to stay well-mixed with the gas when large grains are settling. As a result much of UV radiation important for chemistry is still absorbed in the surface layers of the disk in the settled model. The C^+/C/CO and the O/O_2 transitions thus occur only slightly lower in the disk.
– Dust settling increases the intensity of atomic and molecular lines, and has a subtle influence on the line shapes due to the smaller amount of hot gas, especially at small radii.

Acknowledgements. The authors are grateful to Inga Kamp for many discussions on the thermal balance, and for jointly carrying out a detailed comparison of codes. They thank Michiel Hogerheijde and Floris van der Tak for the use of their 2-D radiative transfer code. This work was supported by a Spinoza grant from the Netherlands Organization of Scientific Research (NWO) and by the European Community's Human Potential Programme under contract HPRN-CT-2002-00308, PLANETS.

References

Aikawa, Y., Umebayashi, T., Nakano, T., & Miyama, S. M. 1997, ApJ, 486, L51
Aikawa, Y., van Zadelhoff, G. J., van Dishoeck, E. F., & Herbst, E. 2002, A&A, 386, 622
Bakes, E. L. O., & Tielens, A. G. G. M. 1994, ApJ, 427, 822

Bary, J. S., Weintraub, D. A., & Kastner, J. H. 2003, ApJ, 586, 1136
Bell, K. R., Cassen, P. M., Klahr, H. H., & Henning, T. 1997, ApJ, 486, 372
Bergin, E., Calvet, N., D'Alessio, P., & Herczeg, G. J. 2003, ApJ, 591, L159
Berruyer, N. 1991, A&A, 249, 181
Black, J. H., & van Dishoeck, E. F. 1987, ApJ, 322, 412
Boss, A. P. 2000, ApJ, 536, L101
Brittain, S. D., Rettig, T. W., Simon, T., et al. 2003, ApJ, 588, 535
Burke, J. R., & Hollenbach, D. J. 1983, ApJ, 265, 223
Chiang, E. I., & Goldreich, P. 1997, ApJ, 490, 368
Costa, V. M., Lago, M. T. V. T., Norci, L., & Meurs, E. J. A. 2000, A&A, 354, 621
D'Alessio, P., Calvet, N., Hartmann, L., Lizano, S., & Cantó, J. 1999, ApJ, 527, 893
D'Alessio, P., Cantó, J., Calvet, N., & Lizano, S. 1998, ApJ, 500, 411
Dartois, E., Dutrey, A., & Guilloteau, S. 2003, A&A, 399, 773
Draine, B. T. 1978, ApJS, 36, 595
Dullemond, C. P., van Zadelhoff, G. J., & Natta, A. 2002, A&A, 389, 464
Dutrey, A., Guilloteau, S., Duvert, G., et al. 1996, A&A, 309, 493
Dutrey, A., Guilloteau, S., & Guelin, M. 1997, A&A, 317, L55
Flower, J. 2001, J. Phys. B, 34, 1
Flower, J., & Launay, J. 1977, J. Phys. B, 10, 3673
Hayes, M. A., & Nussbaumer, H. 1984, A&A, 134, 193
Herczeg, G. J., Linsky, J. L., Valenti, J. A., Johns-Krull, C. M., & Wood, B. E. 2002, ApJ, 572, 310
Hogerheijde, M. R., & van der Tak, F. F. S. 2000, A&A, 362, 697
Hollenbach, D. J., & Tielens, A. G. G. M. 1997, ARA&A, 35, 179
Jansen, D. J., van Dishoeck, E. F., Black, J. H., Spaans, M., & Sosin, C. 1995, A&A, 302, 223
Jaquet, R., Staemmler, V., Smith, M. D., & Flower, D. R. 1992, J. Phys. B, 25, 285
Kamp, I., & Dullemond, C. P. 2004, to be submitted
Kamp, I., & van Zadelhoff, G.-J. 2001, A&A, 373, 641
Kamp, I., van Zadelhoff, G.-J., van Dishoeck, E. F., & Stark, R. 2003, A&A, 397, 1129
Kastner, J. H., Zuckerman, B., Weintraub, D. A., & Forveille, T. 1997, Science, 277, 67
Kenyon, S. J., & Hartmann, L. 1987, ApJ, 323, 714
Koerner, D. W., & Sargent, A. I. 1995, AJ, 109, 2138
Launay, J. M., & Roueff, E. 1977a, A&A, 56, 289
Launay, J. M., & Roueff, E. 1977b, J. Phys. B, 10, 879
Le Bourlot, J., Pineau des Forêts, G., & Flower, D. R. 1999, MNRAS, 305, 802
Li, A., & Greenberg, J. M. 1997, A&A, 323, 588
Lissauer, J. J. 1993, ARA&A, 31, 129
Mannings, V., & Sargent, A. I. 1997, ApJ, 490, 792
Markwick, A. J., Ilgner, M., Millar, T. J., & Henning, T. 2002, A&A, 385, 632
Meeus, G., Waters, L. B. F. M., Bouwman, J., et al. 2001, A&A, 365, 476
Miyake, K., & Nakagawa, Y. 1995, ApJ, 411, 361
Najita, J., Carr, J. S., & Mathieu, R. D. 2003, ApJ, 589, 931
Press, W. H., Flannery, B. P., Teukolsky, S. A., & Vetterling, W. T. 1989, Numerical Recipes – The Art of Scientific Programming (FORTRAN Version) (Cambridge University Press)
Qi, C., Kessler, J. E., Koerner, D. W., Sargent, A. I., & Blake, G. A. 2003, ApJ, 597, 986
Schröder, K., Staemmler, V., Smith, M. D., Flower, D. R., & Jaquet, R. 1991, J. Phys. B, 24, 2487
Shu, F. H., Adams, F. C., & Lizano, S. 1987, ARA&A, 25, 23
Shuping, R. Y., Bally, J., Morris, M., & Throop, H. 2003, ApJ, 587, L109
Stepinski, T. F., & Valageas, P. 1996, A&A, 309, 301
Thi, W. F., van Dishoeck, E. F., Blake, G. A., et al. 2001, ApJ, 561, 1074
Thi, W. F., van Zadelhoff, G. J., & van Dishoeck, E. F. 2004, in press
Throop, H. B., Bally, J., Esposito, L. W., & McCaughrean, M. J. 2001, Science, 292, 1686
Tielens, A. G. G. M., & Hollenbach, D. J. 1985, ApJ, 291, 722
van Dishoeck, E. F., & Black, J. H. 1988, ApJ, 334, 771
van Zadelhoff, G. J., Aikawa, Y., Hogerheijde, M. R., & van Dishoeck, E. F. 2003, A&A, 397, 789
van Zadelhoff, G. J., van Dishoeck, E. F., Thi, W. F., & Blake, G. A. 2001, A&A, 377, 566
Warin, S., Benayoun, J. J., & Viala, Y. P. 1996, A&A, 308, 535
Weidenschilling, S. J. 1997, Icarus, 127, 290
Willacy, K., & Langer, W. D. 2000, ApJ, 544, 903

Online Material

Appendix A: Heating processes

In the following, the various processes included in the calculation of the total heating rate are discussed. Also, their scaling with $m_{\rm gas}/m_{\rm dust}$ is indicated.

Photoelectric heating: the energetic electrons released by absorption of UV photons by dust grains contribute significantly to the total heating rate in the surface of the disk. For the heating rate due to the photoelectric effect the formula by Tielens & Hollenbach (1985) is used:

$$\Gamma_{\rm PE} = 2.7\times10^{-25}\,\delta_{\rm uv}\,\delta_{\rm d}\,n_{\rm H}\,Y\,I_{\rm UV} \times\left[(1-x)^2/x + x_k\left(x^2-1\right)/x^2\right]\ {\rm erg\,cm^{-3}\,s^{-1}}$$

with $\delta_{\rm uv} = 2.2$, $\delta_{\rm d} = 1.25$ and $Y = 0.1$. The strength of the radiation field $I_{\rm UV}$ is calculated with the 2-D Monte Carlo code by van Zadelhoff et al. (2003). x is the grain charge parameter, found by solving the equation

$$x^3 + (x_k - x_d + \gamma)x^2 - \gamma = 0$$

where $x = E_0/E_{\rm H}$, $x_k = kT/E_{\rm H}$, $x_{\rm d} = E_{\rm d}/E_{\rm H}$ and $\gamma = 2.9\times10^{-4}Y\sqrt{T}I_{\rm UV}n_{\rm e}^{-1}$; $E_{\rm H}$ is the ionization potential of hydrogen, $E_{\rm d}$ is the ionization potential of a neutral dust grain (6 eV is assumed here) and E_0 is the grain potential including grain charge effects. This rate is scaled with $m_{\rm dust}/m_{\rm gas}$ to account for the varying gas to dust ratio in models where dust settling was included.

PAH heating: analogous to photoelectric heating, the photoelectrons from PAH ionization also contribute to the heating of the gas. The heating rate described in Bakes & Tielens (1994) is used, using PAHs containing N_C carbon atoms ($30 < N_{\rm C} < 500$). The radiation field used to obtain this heating rate is calculated with the 2-D Monte Carlo code by van Zadelhoff et al. (2003).

C photoionization: it is assumed that each electron released by the photoionization of neutral C delivers approximately 1 eV to the gas. The heating rate then becomes

$$\Gamma_{\rm C\ ion} = 1.7\times10^{-12}\,R_{\rm C\ ion}\,n({\rm C})\,{\rm erg\,cm^{-3}\,s^{-1}}$$

where $R_{\rm C\ ion}$ is the C ionization rate.

Cosmic rays: another source of energetic electrons is the ionization of H and H_2 by cosmic rays. It is assumed that about 8 eV of the electron's energy is used to heat the gas in the case of H_2, and 3.5 eV in the case of H. The H_2 contribution is scaled to include the ionization of He. A cosmic ray ionization rate of $\zeta_{\rm CR} = 5\times10^{-17}\ {\rm s^{-1}}$ is used. The heating rate then becomes

$$\Gamma_{\rm CR} = \left[2.5\times10^{-11}\,n({\rm H_2}) + 5.5\times10^{-12}\,n({\rm H})\right] \times\zeta_{\rm CR}\,{\rm erg\,cm^{-3}\,s^{-1}}$$

H_2 *formation*: of the 4.48 eV liberated by formation of H_2 on dust grains, it is assumed that 1.5 eV is returned to the gas. The corresponding heating rate is:

$$\Gamma_{\rm H_2\ form} = 2.4\times10^{-12}\,R_{\rm H_2\ form}\,n_{\rm H}\,{\rm erg\,cm^{-3}\,s^{-1}}$$

where $R_{\rm H_2\ form} = 3\times10^{-18}\,\sqrt{T}\,n_{\rm H}\,n({\rm H})/(1+T/T_{\rm stick})$ is the H_2 formation rate, with $T_{\rm stick} = 400$ K. This rate is scaled with $m_{\rm dust}/m_{\rm gas}$ in models where dust settling is included.

H_2 *dissociation*: when H_2 is excited into the Lyman and Werner bands, there is about 10% chance that it will decay into the vibrational continuum, thus dissociating the molecule. Each of the H atoms created this way carries approximately 0.4 eV. This gives:

$$\Gamma_{\rm H_2\ diss} = 6.4\times10^{-13}\,n\,({\rm H_2})\ R_{\rm H_2\ diss}\,{\rm erg\,cm^{-3}\,s^{-1}}$$

where $R_{\rm H_2\ diss}$ is the H_2 photodissociation rate.

H_2 *pumping*: electronically excited H_2 that does not disscociate decays into bound vibrationally excited states of the electronic ground state. It is assumed that 2.6 eV is returned to the gas by collisional de-excitations, resulting in:

$$\Gamma_{\rm H_2pump} = 4.2\times10^{-12}\,\left[n({\rm H})\,\gamma_{\rm H} + n\,({\rm H_2})\ \gamma_{\rm H_2}\right] \times n\,({\rm H_2^*})\ {\rm erg\,cm^{-3}\,s^{-1}}$$

where $\gamma_{\rm H}$ and $\gamma_{\rm H_2}$ are the deexcitation rate coefficients through collisions by H and H_2, respectively. These rates are taken from Le Bourlot et al. (1999). H_2^* is calculated explicitly in our models in the UV excitation of H_2.

Chemical heating: in principle every exothermic reaction contributes to the heating of the gas. The reactions considered here (and the energies released) are the dissociative recombination of H_3^+ (in which 9.23 eV is realeased by dissociating to H+H_2 and 4.76 eV by dissociating to H+H+H), HCO^+ (7.51 eV) and H_3O^+ (6.27 eV), and the destruction by He^+ ions of H_2 (6.51 eV) and CO (2.22 eV).

Gas-dust collisions: collisions between gas and dust will heat the gas when the dust temperature is higher than the gas temperature, and will act as a cooling term when the dust temperature is lower than the gas temperature. The formula by Burke & Hollenbach (1983) is used, assuming an average of $\left\langle\sigma_{\rm gr}n_{\rm gr}\right\rangle = 1.5\,n_{\rm H}\ {\rm cm^{-1}}$ and an accomodation coefficient $\bar{\alpha}_T = 0.3$. The resulting rate is scaled with the local value of $m_{\rm dust}/m_{\rm gas}$ in models where dust settling was included:

$$\Gamma_{\rm gd} = 1.8\times10^{-33}\,n_{\rm H}^2\ \sqrt{T}\,(T_{\rm dust}-T_{\rm gas})\,{\rm erg\,cm^{-3}\,s^{-1}}$$

Appendix B: Cooling processes

The gas is cooled through the fine-structure lines of C^+, C and O, and the rotaional lines of CO. For each species the level population was calculated assuming statistical equilibrium:

$$\frac{{\rm d}n_i}{{\rm d}t} = \sum_{j\neq i} n_j\,R_{j\rightarrow i} - n_i\sum_{j\neq i}R_{i\rightarrow j} = 0$$

where n_i is the density of a given species in energy state i, and $R_{i\rightarrow j}$ is the total rate of level i to level j. For all species, collisional excitations and de-excitations are taken into account, as well as spontaneous emission and absorption and stimulated emission through interaction with the cosmic microwave background (CMB) and the dust infrared background. For C^+ and O, UV pumping of the fine-structure lines is also included. Once the populations are known, the cooling rate can be found using the formula by Tielens & Hollenbach (1985):

$$\Lambda_X(\nu_{ij}) = n_i\,A_{ij}\,h\nu_{ij}\,\beta_{\rm esc}(\tau_{ij})\frac{S\,(\nu_{ij})-P(\nu_{ij})}{S\,(\nu_{ij})}.$$

In this formula, n_i is the density of species X in energy state i, A_{ij} is the Einstein A coefficient for the transition $i \rightarrow j$, ν_{ij} is the corresponding frequency, and $\beta_{\rm esc}(\tau_{ij})$ is the escape probability at optical depth τ_{ij}. $S(\nu_{ij})$ is the local source function:

$$S(\nu_{ij}) = \frac{2h\nu_{ij}^3}{c^2}\left(\frac{g_i n_j}{g_j n_i} - 1\right)^{-1}$$

where g_i is the statistical weight of level i. $P(\nu_{ij})$ is the intensity of the background radiation:

$$P(\nu_{ij}) = B_{\nu_{ij}}(T_{\rm CMB}) + \tau_{\rm dust} B_{\nu_{ij}}(T_0)$$

where $T_{\rm CMB}$ is the temperature of the cosmic background (2.726 K) and T_0 the characteristic temperature of the dust at the surface of the disk. In the calculation of the collision rates of all cooling species considered here, the ortho/para ratio for H_2 was assumed to be in thermal equilibrium with the local gas temperature.

O cooling: O contributes to the cooling of the gas in the surface layers of the disk through its fine-structure lines at 63.2 μm and 145.6 μm. The Einstein A coefficients for these lines are 8.87×10^{-5} s^{-1} and 1.77×10^{-5} s^{-1}, respectively. Collisions with electrons (Hayes & Nussbaumer 1984), H (Launay & Roueff 1977a) and H_2 (Jaquet et al. 1992) were included. O can also act as a heating agent if infrared pumping is followed by collisional de-excitation. If that happens the cooling rate becomes negative and is treated as a heating rate by the code. This phenomenon did not occur in the calculations presented in this paper.

C^+ *cooling*: C^+ contributes to the cooling of the gas through its fine-structure line at 158 μm. An Einstein A coefficient of 2.29×10^{-6} s^{-1} is used. Collisions with electrons (Hayes & Nussbaumer 1984), H (Launay & Roueff 1977b) and H_2 (Flower & Launay 1977) are included in calculating the level populations.

C cooling: C cools the gas through its fine-structure lines at 370 μm and 609 μm. The Einstein A coefficients used are 2.68×10^{-7} s^{-1} and 7.93×10^{-8} s^{-1}, respectively. Collisions with H (Launay & Roueff 1977a) and H_2 (Schröder et al. 1991) are included.

CO cooling: CO is the main coolant of the dense, shielded regions deep in the disk through its rotational lines. The 20 lowest rotational transitions of CO are included in the model. The Einstein A coefficients used in this work are identical to those adopted by Kamp & van Zadelhoff (2001). Collisions with H (Warin et al. 1996) and H_2 (Flower 2001) are taken into account to calculate the populations.